Dalton Transactions

Multifaceted Sn–Sn bonding in the solid state. Synthesis and structural characterization of four new Ca–Li–Sn compounds

Journal:	*Dalton Transactions*
Manuscript ID	DT-ART-07-2019-002803.R1
Article Type:	Paper
Date Submitted by the Author:	23-Aug-2019
Complete List of Authors:	Ovchinnikov, Alexander; University of Delaware Bobev, Svilen; University of Delaware, Chemistry and Biochemistry

Dalton Transactions

ARTICLE

Multifaceted Sn–Sn bonding in the solid state. Synthesis and structural characterization of four new Ca–Li–Sn compounds

Received 00th January 20xx,
Accepted 00th January 20xx

DOI: 10.1039/x0xx00000x

www.rsc.org/

Alexander Ovchinnikov,[a,b] and Svilen Bobev*[a]

Four novel ternary phases have been prepared in the system Ca–Li–Sn using both the metal flux method and conventional high-temperature synthesis. Each of the obtained compositions represents its own (new) structure type, and the structures feature distinct polyanionic Sn units. Ca_4LiSn_6 (space group *Pbcm*, Pearson symbol *oP*44) accommodates infinite chains, made up of cyclopentane-like [Sn_5]-rings, which are bridged by Sn atoms. All Sn atoms in this structure are two-bonded. The anionic substructure of $Ca_9Li_{6+x}Sn_{13-x}$ ($x \approx 0.28$, space group *C*2/*m*, Pearson symbol *mS*56) displays extensive mixing of Li and Sn and combination of single-bonded and hypervalent interactions between the Sn atoms. Hypervalent bonding is also pronounced in the structure of the third compound, Ca_2LiSn_3 (space group *Pmm*2, Pearson symbol *oP*18) with quasi-two-dimensional polyanionic subunits and a variety of coordination environments of the Sn atoms. One-dimensional [Sn_{10}]-chains with intricate topology of *cis*- and *trans*-Sn–Sn bonds exist in the structure of $Ca_{9-x}Li_2Sn_{10}$ ($x \approx 0.16$, space group *C*2/*m*, Pearson symbol *mS*42), and the Sn–Sn bonding in this case demonstrates the characteristics of intermediate between single- and double- bond-order. The peculiarities of the bonding are discussed in the context of the Zintl approach, which captures the essence of the main chemical interactions. The electronic structures of all four compounds have also been analyzed in full detail using first-principle calculations.

Introduction

Efficiency in energy storage is one of the key objectives in today's materials science. One of the most actively developing directions in this domain is electrochemical power sources. Among numerous designed devices, Li-ion batteries have gained the highest recognition and widest practical application in the modern technologies. Current transition-metal-oxide-based electrode materials in such batteries suffer from several drawbacks, such as poor mechanical stability, low charging rates and potentially hazardous environmental impact.[1] Therefore, development of new electrode materials that will lack these shortcomings is indispensable.

Examples of non-oxide electrode materials that have been studied in the recent years include metal compounds with the elements of group 16, 15, and 14 in the Periodic table (the elements referred to as chalcogenes, pnictogens, and tetrels, respectively).[2] In particular, recent investigations of clathrate materials based on group 14 elements showed promising results with respect to performance in Li-ion-based electrochemical energy storage applications.[3] Our studies in this field indicated that the behavior of clathrates upon lithiation strongly depends on the valence electron count and the nature of the tetrel element constituting the framework.[4,5] So far, we have mainly focused our attention on silicon and germanium-based systems. However, compounds of the heavier congeners, i.e. tin and lead, may also be of interest, since the materials containing these elements typically display higher electrical conductivities than silicides and germanides. In addition, the higher metallicity of stannides and plumbides provides better mechanical properties upon electrochemical cycling due to inherently higher expandability of metals. Although high atomic weights of Sn and Pb are detrimental to the electrochemical capacity, the often unique crystal structures of their compounds may yield materials with interesting electrochemical properties.

Binary transition metal stannides have been previously studied as potential electrodes for rechargeable Li-ion batteries. For instance, $CrSn_2$ and $CoSn_2$ have been reported to get reduced to elemental metals upon Li insertion, which results in decreased discharge capacities after the first cycle.[6] In contrast, lithiation of Cu_6Sn_5 is believed to yield the ternary zincblende-type phase Li_2CuSn, which can be reversibly delithiated.[7,8] In certain cases, chemical processes accompanying electrochemical cycling have not been fully established. For example, reversible lithiation has been observed for the binary Ni stannide Ni_3Sn_2.[9] However, the nature of the lithiated product has never been determined.

[a] Department of Chemistry and Biochemistry, University of Delaware, Newark, Delaware 19716, United States
[b] Department of Materials and Environmental Chemistry, Stockholm University, Stockholm 10691, Sweden

† Electronic Supplementary Information (ESI) available: PXRD patterns, plots of local coordination environments of the Li atoms, addition plots of DOS, selected interatomic distances. CIFs from all refined structures have been deposited with the Cambridge Structural Database (CSD) of X-ray structural data and have access codes CCDC 1938687-1938690. See DOI: 10.1039/x0xx00000x

In general, detailed structural studies of the phases forming upon electrochemical cycling are often complicated due to amorphization of the Li-intercalated products and their tendency to segregate at the interfaces rather than in the form of bulk materials. To circumvent these difficulties, it is desirable to establish the structures of all possible Li-containing phases in the studied systems beforehand, using high-quality crystalline materials. After the compositions and structures of these phases have been ascertained, the nature of the lithiated products prepared in *operando* conditions can be revealed by comparing the available analytical data, collected *in situ* or after electrochemical treatment, with those of the previously characterized bulk compounds.

Following our successful synthesis of the new quaternary Li-bearing germanides $AELi_2In_2Ge_2$ (*AE* = Sr, Ba, Eu) using a metal flux approach,[10] we started exploration of similar intermetallic systems containing a heavier germanium congener, tin. The latter can be efficiently used as a flux due to its low melting point (T_m = 505 K), wide temperature range of the liquid phase existence (boiling point T_b = 2873 K), and high solubility of many metals in molten tin. Combination of tin with electropositive elements, e.g., alkaline-earth metals, frequently yields compounds displaying polyanionic structural units with extended Sn–Sn bonding. Imaginary formation of such units from isolated anionic Sn^{4-} species can be formally regarded as chemical oxidation, whereas cleavage of the homoatomic Sn–Sn bonds corresponds to chemical reduction. This structural variability may potentially lead to materials that can be reversibly reduced or oxidized (e.g., upon lithium intercalation or extraction) if these processes are coupled to concomitant changes of some of the Sn–Sn interactions, respectively, providing that the average crystal structure is retained.

Our preliminary synthetic attempts were carried out in the Ca–Li–Sn system, where four ternary phases have been reported so far—CaLiSn,[11] $Ca_7Li_5Sn_{11}$,[12] $Ca_9Li_{9-x}Sn_{6+x}$,[12] and $CaLi_2Sn$.[13] Our first flux growth experiments produced two new ternary compounds, Ca_4LiSn_6 and $Ca_9Li_{6+x}Sn_{13-x}$. Subsequent reactions employing conventional high-temperature annealing of the elements yielded two more phases, which also have not been described before, Ca_2LiSn_3 and $Ca_{9-x}Li_2Sn_{10}$. With the four newly discovered representatives, each crystallizing in its own and unprecedented structure type, we were able to double the number of ternary phases in the apparently well-studied Ca–Li–Sn system. The crystal structures of these novel compounds demonstrate various sorts of polyanionic building blocks with homoatomic Sn–Sn interactions of different kinds, as was revealed by our first-principle calculations.

Results and discussion

Crystal structure

Ca_4LiSn_6. Irregularly shaped single crystals of Ca_4LiSn_6 could easily be distinguished from the cubic crystals of the major phase $CaSn_3$,[14] which forms readily under Sn-flux conditions. Indexing of the single-crystal diffraction patterns yielded an orthorhombic unit cell with *a* = 9.2035(4) Å, *b* = 8.8019(5) Å, *c* = 14.9400(8) Å. Crystal structure solution was successful in space group *Pbcm* (# 57, Fig. 1a) and provided positions for all Ca and Sn atoms. The Li atoms were located from difference Fourier mapping. The subsequent refinement was straightforward. All atoms including Li were refined anisotropically. Anisotropic displacement parameters (ADPs) for one of the tin sites (Sn4) were found to be somewhat higher in comparison with the other Sn atoms (see Table 2), due to the location of this site in a bridging position (see below). Independent refinements of the atomic occupation parameters converged to 100 % occupancy within several standard deviations, suggesting that the discussed compound is devoid of disorder.

The main structural feature in Ca_4LiSn_6 is chains of pentagonal Sn_5 rings connected by bridging Sn atoms. The chains propagate along the *c*-axis, whereas the rings are stacked along the *b* direction with a small tilt with respect to the crystallographic axis. Similar cyclic Sn_5 units were previously reported in the crystal structures of some other stannides: Na_8AESn_6 (*AE* = Ba, Eu),[15] $AELi_{9-x}Sn_{6+x}$ (*AE* = Ca, Eu), $Eu_5Li_6Sn_9$, and $Ca_7Li_5Sn_{11}$.[12] In these compounds, planar isolated [Sn_5] units are present, which can be regarded as all-inorganic aromatic species with a formal charge of "6–". In contrast to such moieties, the Sn_5 fragments in Ca_4LiSn_6 adopt a nonplanar shape similar to the envelope conformation of a cyclopentane molecule, suggesting that no delocalized π-bonding is taking place in this case. The Sn–Sn contacts within the rings, ranging from 2.7971(5) Å to 2.9634(3) Å, as well as the contact between the rings and the adjacent bridging Sn atoms (d_{Sn-Sn} = 2.9981(3) Å), should therefore be considered as single bonds. Similar interatomic distances between Sn atoms are also found in other compounds with single-bonded Sn–Sn contacts.[16] The Li atoms cap the pentagonal rings with the corresponding Li–Sn contacts ranging from 2.891(8) Å to 3.096(6) Å.

According to the Zintl concept, which is widely used to rationalize structures and compositions of such compounds,[17–21] an isolated Sn atom must have a formal charge of "4–" in order to achieve its stable (filled) octet electron configuration. Accordingly, a single-bonded Sn atom is assigned a formal charge of "3–", whereas formal charges of "2–", "1–", and "0" are ascribed to tin atoms having two, three, or four covalent bonds, respectively. In the structure of Ca_4LiSn_6, there is one Sn atom with three Sn–Sn bonds around it (the Sn1 position in the rings, directly connected to two Sn-atom neighbors in the ring and to the Sn4 atom in bridging position). The remaining three symmetrically independent tin sites are two-bonded (Sn2 and Sn3 participate in bonding in the rings only and Sn4 is the aforementioned bridging atom). The highly polar Ca–Sn and Li–Sn interactions are not viewed as covalent bonds and are omitted from these considerations. Taking into account the multiplicities of the Sn sites, the partitioning of the valence electrons in Ca_4LiSn_6 can be expressed in the following manner: $(Ca^{2+})_4(Li^+)(Sn^{1-})_2(Sn^{2-})_4(h^+)$, where h^+ denotes an electron hole. According to this description, the composition appears to be one-electron-short of the optimal electron

count. This conclusion is corroborated by our first-principle calculations, detailed in the following section.

$Ca_9Li_{6+x}Sn_{13-x}$ ($x \approx 0.28$). Similarly to the case of Ca_4LiSn_6, the crystals of $Ca_9Li_{6+x}Sn_{13-x}$ ($x \approx 0.28$) were first isolated from the sample mainly consisting of the binary $CaSn_3$ phase. The initial structural model in space group *C*2/*m* (# 12, Fig. 1b) was augmented by adding Li atoms found after difference Fourier mapping. For the final anisotropic refinement, introduction of mixed Li/Sn occupancy was necessary to account for the observed residual electron density and anomalies of the anisotropic displacement parameters. The two mixed-occupied sites (Li/Sn)3 and (Li/Sn)4 have the refined Li/Sn ratios of about 0.45/0.55 and 0.69/0.31, respectively. In many other ternary and quaternary phases, Li has also been observed to partially substitute for p-elements, such as Ga,[22] In,[22,23] and Sn.[24] For the sake of brevity and simplicity, in the next paragraphs, these positions will be referred to as Li3 and Li4, respectively. We will also note here that one of Li sites (Li2), which does not appear to be admixed with Sn, displays an elongated thermal ellipsoid. Although this may be partially related to the known difficulties of refining Li coordinates and ADPs in the presence of heavy atoms, this may also hint toward possible mobility of Li in these positions, as in the reported structure of the electrochemically active $Li_{17}Sn_4$.[25,26]

It is convenient to describe the anionic structure of $Ca_9Li_{6+x}Sn_{13-x}$ ($x \approx 0.28$) as consisting of two types of principal building blocks. The first type is comprised of interlinked Li3- and Li4-centered tetrahedra. They share common corners in two orthogonal directions. In the *ac*-plane, the terminal Sn4 and Sn5 atoms from adjacent tetrahedra come in proximity of each other (d_{Sn-Sn} = 2.865(1) Å) and form a Sn–Sn dumbbell. Altogether, the two types of corner-shared tetrahedra form chains running along the crystallographic *b*-direction. These chains are interconnected pair-wise by the dumbbells. This mode of interlinking produces flat pentagonal rings composed of Sn and Li/Sn, stacked along the *b*-axis in the eclipsed orientation, with some of the Ca atoms (Ca2) occupying the spaces between the rings. A similar structural motif with alternating isolated aromatic $[Sn_5]^{6-}$ units and cations of electropositive metals has been observed in the already mentioned compounds Na_8AESn_6 (*AE* = Ba, Eu),[15] $AELi_{9-x}Sn_{6+x}$ (*AE* = Ca, Eu), $Eu_5Li_6Sn_9$, and $Ca_7Li_5Sn_{11}$.[12] The Li–Sn and Sn–Sn distances within the double chains in the structure of $Ca_9Li_{6+x}Sn_{13-x}$ ($x \approx 0.28$) are in the range 2.797(2)– 2.9036(9) Å,

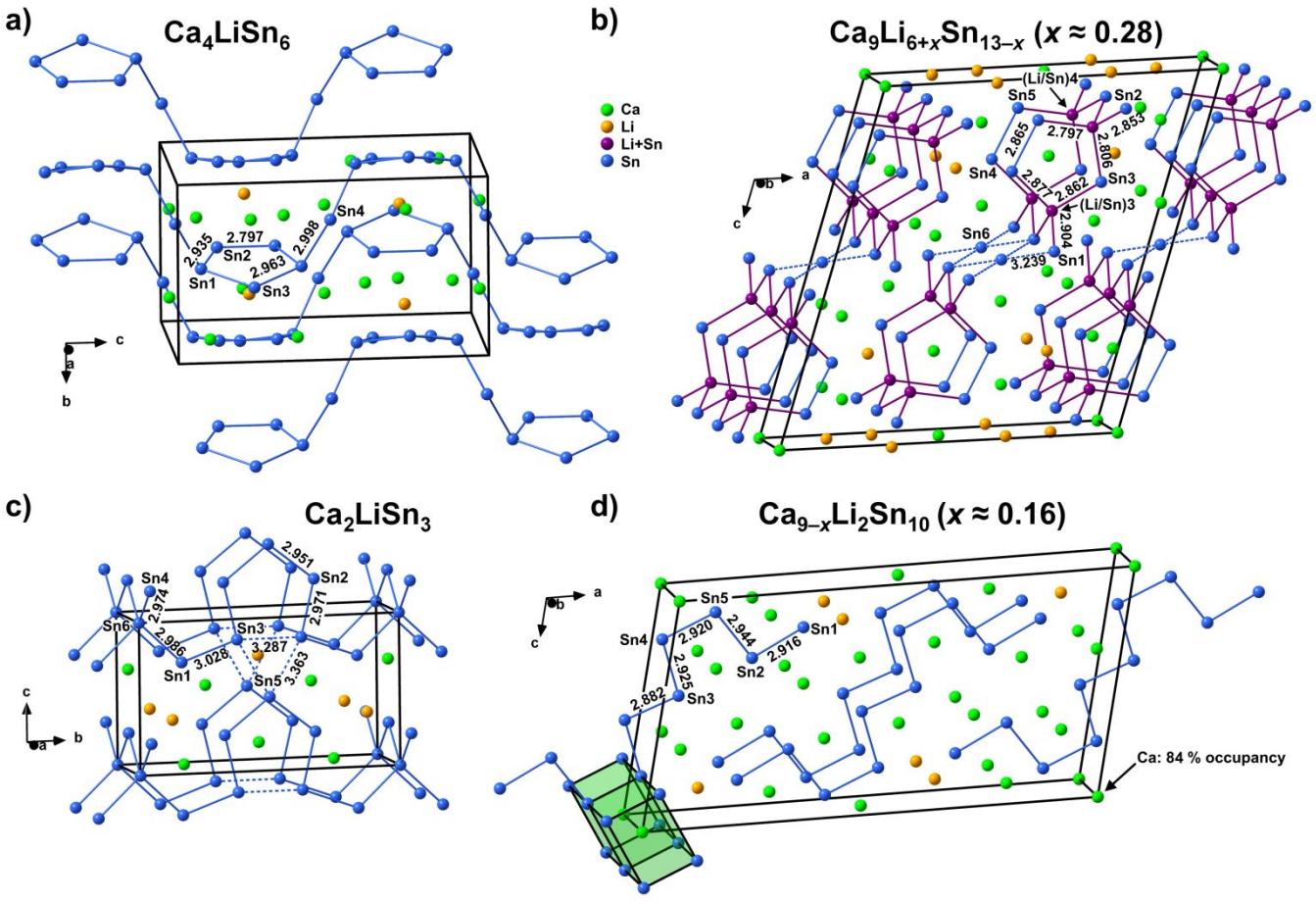

Figure 1. Crystal structures of Ca_4LiSn_6 (a), $Ca_9Li_{6+x}Sn_{13-x}$ ($x \approx 0.28$) (b), Ca_2LiSn_3 (c), and $Ca_{9-x}Li_2Sn_{10}$ ($x \approx 0.16$) (d). Symmetrically unique tin atoms and mixed-occupied Li/Sn sites are labeled. The coordination environments of the Ca atoms are not shown for clarity, except of the partially occupied Ca5 site in $Ca_{9-x}Li_2Sn_{10}$ ($x \approx 0.16$) (d), which is indicated. Relevant distances are given (in Å). Unit cells are outlined in black.

which agrees well with the sum of the single-bonded radii and matches the reported values for Sn–Sn bond lengths, as well as Li–Sn distances, found in other stannides.[16,24]

The second kind of anionic building block in $Ca_9Li_{6+x}Sn_{13-x}$ ($x \approx 0.28$) can be described as columns of Sn atoms (Sn6) residing between the above-described double chains along the *b*-axis. These Sn atoms are located in the centers of distorted squares formed by the Sn1 atoms from the surrounding chains. The Sn6–Sn1 distance of 3.2390(6) Å is much longer than typical Sn–Sn single bonds. However, similarly long homoatomic contacts in stannides have been designated in the literature as hypervalent, i.e. electron-rich, interactions.[27,28] Within the frame of this description, the long Sn6–Sn1 contact can be viewed as a one-electron bond. Using the same formalism for calculating charges on Sn atoms, as done previously for the Ca_4LiSn_6 example, a tin atom with one one-electron bond can be assigned a formal charge of "3.5–" (owing to the sharing of one electron between two bonded atoms), and every extra bond of this kind adds a charge of "0.5+", whereas a regular two-electron bond provides an extra charge of "1+".

Notwithstanding the complex crystal structure and occupational disorder, the chemical bonding in this unusual stannide can be rationalized using the Zintl approach too. By considering the number of two-center and one-center Sn–Sn bonds around the tin species in the structure and taking into account the statistical distribution of tin in the mixed-occupied sites, the following formal charges can be assigned: $Sn1^{(0.55\cdot1-\,+\,0.45\cdot3-)}$, $Sn2^{2-}$, $Sn3^{2-}$, $Sn4^{(0.55\cdot2-\,+\,0.45\cdot3-)}$, $Sn5^{(0.31\cdot2-\,+\,0.69\cdot3-)}$, $Sn6^{2-}$. The tin atoms occupying the tetrahedral sites together with Li have zero formal charges, since they are four-bonded. The overall accounting of the electrons can be then summarized with the formula $(Ca^{2+})_9(Li^{+})_{6.28}(Sn_{12.72})^{24.08-}(e^{-})_{0.2}$. This means that the refined composition corresponds to nearly complete electron-balanced one—there are only ca. 0.2 electrons in excess per formula unit. Apparently, the observed Li/Sn mixing is an important electronic structure-stabilizing factor, which drives the system toward electron-precise formulation, thereby optimizing the chemical bonding. On that note, it is important to add that refinement of the mixed atomic sites as partially occupied by Sn does result in a comparable fitting quality. However it produces a tin-deficient structure, which appears to be two-electrons-short. In addition, missing Sn atoms would perturb the strong bonding interactions in the polyanion, found in our calculations (see below), suggesting that defects in the Sn sites are not energetically favored.

Ca_2LiSn_3. Although the powder sample with the nominal composition Ca_2LiSn_3 appeared well-crystalline upon a visual inspection, finding single crystals suitable for structural studies proved to be challenging. Most of the tested crystals turned out to be intergrowths or twins with strongly overlapping domains. The best crystal, although of mediocre quality, allowed structure solution in the noncentrosymmetric space group *Pmm*2 (# 25, Fig. 1c). Attempts to solve the structure in a centrosymmetric space group or to derive higher symmetry from the proposed structural model failed. Missing symmetry checks with ADDSYM[29] or FINDSYM[30] did not reveal unaccounted symmetry elements. Furthermore, the intensity statistics favored an acentric space group with $|E^2-1| = 0.709$ (for an ideal acentric structure, this indicator equals 0.736, whereas for a centrosymmetric structure, it is 0.968). It is also worth noting that the unit cell displays pseudo-hexagonal metrics ($b/c = 1.74 \approx \sqrt{3}$), which may (in part) be responsible for the twinning (or rather trilling) problems observed for the majority of the tested crystals. No reasonable structure solution can be obtained by transforming the original pseudo-hexagonal cell in the hexagonal setting. After the positions of the heavy atoms were determined, the Li atoms were located from difference Fourier mapping. However, in contrast to the structures described above, anisotropic refinement for the Li sites was unsuccessful, likely due to the relatively poor crystal quality. Furthermore, one of the two Li sites (Li1) showed an unphysically low isotropic displacement parameter, which could not be fixed by the introduction of twinning or by considering mixed occupation of this position. Therefore, the isotropic displacement parameters were kept equal for the two Li sites and treated as one refinable parameter. The value of the refined Flack's parameter was 0.06(9), asserting the correct absolute configuration for the derived structural model.

The anionic substructure in Ca_2LiSn_3 consists of Sn-centered tetrahedra, which share common vertices and are linked into chains propagating along the *a*-axis. These fragments are connected by bridging Sn_5 pentagonal rings along the *b* direction, thus creating a quasi-two-dimensional structure. The lack of center of symmetry in the structure is not simply due to a small distortion from a hypothetical centrosymmetric prototype, but results from a special, polar atomic packing, which leads, in particular, to the same orientation of the pentagonal rings along the *c*-direction in the Sn layers (Fig. 1c). The two symmetrically unique Sn–Sn contacts in the tetrahedra measure 2.974(3) Å and 2.986(2) Å, indicating covalent bonding. We caution that the given structure description based on $[Sn_5]$-rings should be used with care, since the said $[Sn_5]$-fragments have one long edge. Specifically, four of the bonds within the $[Sn_5]$-units are 2.951(2) Å (×2) and 2.971(3) Å (×2) long, while the last one shows a Sn–Sn distance, which is 3.287(3) Å long. The latter value points toward hypervalent bonding, again. Such Sn–Sn bond can be regarded as an one-electron interaction, drawing from the discussion above on Sn–Sn bonding within the square planar fragments in $Ca_9Li_{6+x}Sn_{13-x}$ ($x \approx 0.28$). With this in mind, the following formal charges for the Sn atoms can be calculated: $Sn1^{2-}$, $Sn2^{2-}$, $Sn3^{1.5-}$, $Sn4^{2-}$, $Sn5^{2-}$, $Sn6^{0}$. The charge accounting derived from this assignment is consistent with the electron-precise notation $(Ca^{2+})_6(Li^{+})_3(Sn^{0})(Sn^{1.5-})_2(Sn^{2-})_6$. However, this description appears to be oversimplified, as another possible interaction can be detected in the structure: The columns of ecliptically stacked $[Sn_5]$-rings running along the *a* direction are located at a relatively short distance, resulting in a separation of 3.363(3) Å between the corners of adjacent rings. Although this distance is even longer than typical hypervalent Sn–Sn bonds, the first-principle calculations provide evidence for a

non-negligible bonding interaction associated with this contact (vide infra).

In addition to the sample prepared according to the optimized procedure, powder X-ray diffraction confirmed the presence of the Ca_2LiSn_3 phase in samples with nominal compositions "Ca_4LiSn_6" (aimed at the phase with the given formula) and "$Ca_9Li_4Sn_{15}$" (aimed at the hypothetical composition $Ca_9Li_{6+x}Sn_{13-x}$ with $x = -2$), prepared following the same experimental protocol used for Ca_2LiSn_3. The peak positions for the Ca_2LiSn_3 phase were consistent with those in the phase-pure sample, and corresponded well with the lattice parameters derived from the single-crystal data. This finding suggests that Ca_2LiSn_3 is likely a line compound.

$Ca_{9-x}Li_2Sn_{10}$ ($x \approx 0.16$). The crystal structure solution and refinement for $Ca_{9-x}Li_2Sn_{10}$ ($x \approx 0.16$) were done in space group *C*2/*m* (# 12, Fig. 1d). The initially obtained model with the composition $Ca_9Li_2Sn_{10}$ showed large anisotropic displacement parameters for the Ca atoms in 2*a* position (Ca5) and a significant negative residual peak in the Fourier synthesis at the same site. These issues were resolved by refining the Ca occupancy, which converged to around 84 %, resulting in the composition $Ca_{9-x}Li_2Sn_{10}$ ($x \approx 0.16$). The Ca deficiency was found in all tested crystals of this phase, including those recovered from samples of different nominal compositions. It is worthwhile to mention that some Ca/Li disorder could potentially account for the reduced electron density in the discussed position. However, such scenario can be safely ruled out, as the two symmetrically unique distances from this site to the adjacent Sn atoms measure 3.3381(3) Å and 3.4356(3) Å, both being far longer than any reported Li–Sn bonding contacts. Our first-principle calculations do not provide any electronic reason for the observed deviation from the ideal $Ca_9Li_2Sn_{10}$ formula. Entropy factors may be at play in this case. The following Ca-centered Sn polyhedra can be easily distinguished in the structure, with the corresponding volumes given in parentheses: [Ca1]Sn_7 (46.22 Å^3), [Ca2]Sn_8 (47.68 Å^3), [Ca3]Sn_7 (47.66 Å^3), [Ca4]Sn_6 (34.56 Å^3), [Ca5]Sn_8 (53.18 Å^3). From these data, it is evident that removal of Ca5 creates the largest free volume. In addition, face-sharing of the distorted Ca5-Sn_8 cubes, stacked along the *b*-axis (Fig. 1(d)), must facilitate Ca diffusion through the structure, which could be responsible for the observed deficiency. As can be concluded from the single-crystal diffraction data on several crystals, the homogeneity range in $Ca_{9-x}Li_2Sn_{10}$ is likely quite narrow, though further studies are necessary to determine the exact extent thereof.

The anionic structure in $Ca_{9-x}Li_2Sn_{10}$ ($x \approx 0.16$) does not contain any pentagonal fragments, observed in other compounds reported here. It bears isolated one-dimensional [Sn_{10}]-chains with intricate topology of *cis*- and *trans*-Sn–Sn bonds instead. Such chains can be viewed as oligomeric fragments cleaved from the infinite chains in the structure of $Eu_5Li_6Sn_9$.[12] In the latter phase, the planarity of the chains was ascribed to a π-bonding contribution. In $Ca_{9-x}Li_2Sn_{10}$ ($x \approx 0.16$), the lengths of the homoatomic Sn–Sn contacts range from 2.8823(5) Å to 2.9437(4) Å, with the shortest bond between the Sn3 atoms in the middle of the chain. Although these contacts can be considered to be single bonds based on the atomic radius (r_{Sn} = 1.41 Å[31]), distances alone may not be reliable bond-order indicators for intermetallic compounds where the chemical bonding is typically with a high degree of delocalization. If all Sn–Sn contacts in the [Sn_{10}]-chains are treated as single bonds, an overall formal charge of "22–" per chain can be calculated, and the following charge partitioning results: $(Ca^{2+})_9(Li^+)_2(Sn^{2-})_8(Sn^{3-})_2(h^+)_2$. This is suggestive of a shortage of two electrons with respect to a fully charge-balanced state. If the Sn3–Sn3 bond (the shortest, 2.8823(5) Å) is presumed to be a double bond, the composition appears to be electron-precise, according to the following breakdown: $(Ca^{2+})_9(Li^+)_2(Sn^{1-})_2(Sn^{2-})_6(Sn^{3-})_2$. In agreement with this line of thinking, if one were to consider a higher proportion of π-bonding involved, the composition would be electron-rich. The example of $Ca_{9-x}Li_2Sn_{10}$ is reminiscent of the barium magnesium silicide $Ba_2Mg_3Si_4$ with planar Si_6 chains (along with Si_2 dumbbells).[32] Electronic structure calculations for the latter compound show an intermediate character of the Si–Si bonding in the chains. Although the treatment of all homoatomic bonds as single in this phase results in a charge-balanced composition $(Ba^{2+})_4(Mg^{2+})_6[(Si^{2-})_4(Si^{3-})_2][(Si^{3-})_2]$, the location of the Fermi level above the pseudo-gap suggests a partial contribution of double-bonding, which would also explain the planarity of the anionic chains. As suggested by our first-principle calculations, a similar situation is realized in $Ca_{9-x}Li_2Sn_{10}$ ($x \approx 0.16$), as will be discussed in the following section.

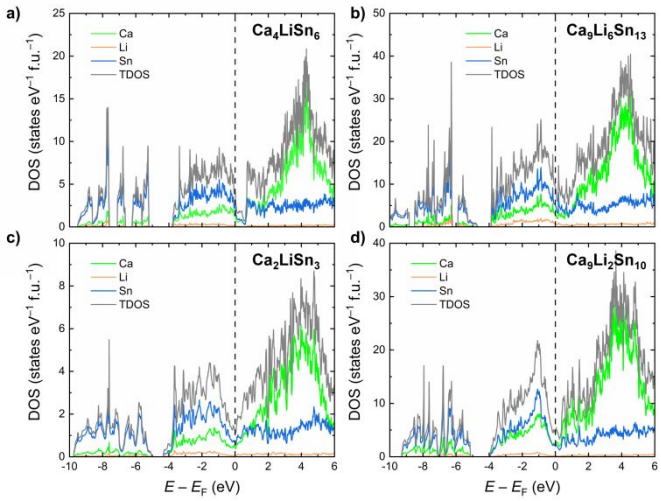

Figure 2. Total and projected electronic densities of states (DOS) for Ca_4LiSn_6 (a), $Ca_9Li_6Sn_{13}$ (b), Ca_2LiSn_3 (c), and $Ca_9Li_2Sn_{10}$ (d).

Electronic structure and chemical bonding

Electronic densities of states (DOS) for Ca_4LiSn_6, idealized $Ca_9Li_{6+x}Sn_{13-x}$ model with the composition $Ca_9Li_6Sn_{13}$, Ca_2LiSn_3, and hypothetical deficiency-free $Ca_9Li_2Sn_{10}$ are shown in Fig. 2a–d, respectively. For the calculations, experimentally determined lattice parameters and atomic coordinates were used. Crystal Orbital Hamilton Population curves (COHP) for the Sn–Sn interactions averaged over symmetrically independent contacts are depicted in Fig. 3. Selected sections

of the crystal structures and Electron Localization Function (ELF) are given in Fig. 4.

In the electronic structures of all four studied models, a sizeable hybridization of the Ca, Li, and Sn states is observed at the Fermi level (E_F) and below, in the region –4 eV < $E - E_F$ < 0 (Fig. 2a–d). In the energy interval –10 eV < $E - E_F$ < –5 eV, the electronic states have a predominant contribution of Sn(5s), reflecting the electronic lone pairs on the Sn atoms.

The electronic spectrum of Ca_4LiSn_6 displays a pronounced pseudogap around $E - E_F \approx 0.6$ eV (Fig. 2a). The location of this feature corresponds to one extra electron per formula unit, thus corroborating the previously proposed notation $(Ca^{2+})_4(Li^+)(Sn^{2-})_4(Sn^{1-})_2(h^+)$. Departure from ideal charge balance is not rare in compounds of the group 14 elements, and was reported, in particular, for silicon and germanium clathrates. In such compounds, the Fermi level is located deeper in the valence band (electron shortage), or is shifted higher into the conduction band (electron excess), with respect to the electronic bandgap.[33,34] Considering the similar atomic radii of Li and Mg, it is possible to envision the electronically-balanced but yet undiscovered composition Ca_4MgSn_6 with the same crystal structure. The Sn–Sn interactions in Ca_4LiSn_6 are almost optimized at E_F with only a minor population of antibonding states (Fig. 3a). The ELF distribution clearly shows maxima between the adjacent Sn atoms in the Sn_5 rings and between the rings and the bridging Sn atoms, confirming strong covalent interactions (Fig. 4a).

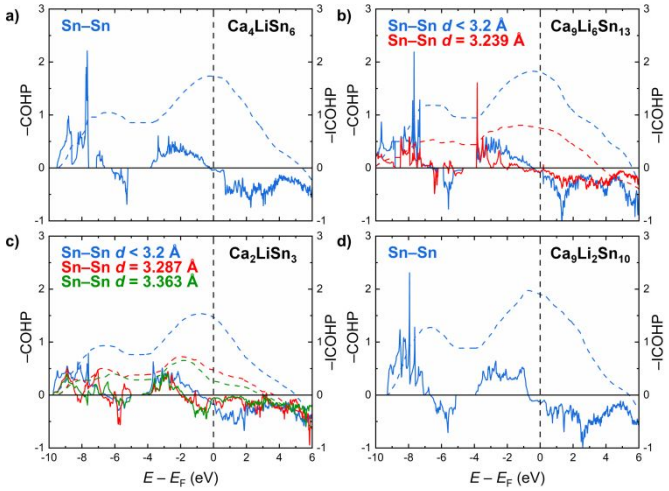

Figure 3. Crystal Orbital Hamilton Population curves (COHP) and their integrals for the selected Sn–Sn contacts in Ca_4LiSn_6 (a), $Ca_9Li_6Sn_{13}$ (b), Ca_2LiSn_3 (c), and $Ca_9Li_2Sn_{10}$ (d).

Calculations on the experimentally observed $Ca_9Li_{6+x}Sn_{13-x}$ ($x \approx 0.28$) composition could not be performed due to the extensive disorder in the structure. Therefore, an idealized model was generated, with (Li/Sn)3 position of the original structure treated as occupied by a Sn atom (below labeled as Sn*) and the original (Li/Sn)4 as occupied by a Li atom (Li4). Although the compositional difference between the refined structure and the employed model is not large, the electronic balance achieved due to the occupational disorder in $Ca_9Li_{6+x}Sn_{13-x}$, is not reflected in the electronic structure of $Ca_9Li_6Sn_{13}$. Indeed, employing the same electron counting approach used for $Ca_9Li_{6+x}Sn_{13-x}$, the following formal charges can be derived: $Sn1^{1-}$, $Sn2^{4-}$, $Sn3^{3-}$, $Sn4^{2-}$, $Sn5^{3-}$, $Sn6^{2-}$, Sn^{*0}. The $Ca_9Li_6Sn_{13}$ model should then follow the notation $(Ca^{2+})_9(Li^+)_6(Sn_{13})^{28-}(h^+)_4$. The electron count in our idealized model appears to differ from that of the refined structure beyond the tolerance of the rigid band approximation, resulting in relatively high DOS values in a wide energy span around the Fermi level, with no discernible (pseudo)gaps. Nevertheless, our model can be used to analyze local electronic features, e.g., chemical bonding. The COHP analysis indicates that the short Sn–Sn interactions (d_{Sn-Sn} < 3.2 Å) demonstrate features similar to Ca_4LiSn_6, being nearly perfectly optimized at the Fermi level (Fig. 3b). The long Sn–Sn contact (d_{Sn-Sn} = 3.239 Å) is hallmarked by an extended region of antibonding states below E_F, down to approximately $E - E_F$ = –1 eV. The overall contribution of these states is relatively small, as high peaks of bonding character are located well below E_F, resulting in an overall bonding situation at the Fermi level. However, the negative integrated COHP value for this contact at E_F (–ICOHP = 0.75 eV/bond) appears to be about two and a half times smaller than the average magnitude for the rest of the symmetrically unique Sn–Sn bonds (<–ICOHP> = 1.80 eV/bond). The described behavior is characteristic for hypervalent bonding interactions,[28,35,36] and confirms that their treatment as one-electron bonds should be applicable. This conclusion is further corroborated by the ELF calculation (Fig. 4b). Whereas the short Sn–Sn contacts reveal clear ELF maxima between the Sn atoms, the longer contact between Sn1 and Sn6 does not display any pronounced covalency, i.e., localization of electron pairs.

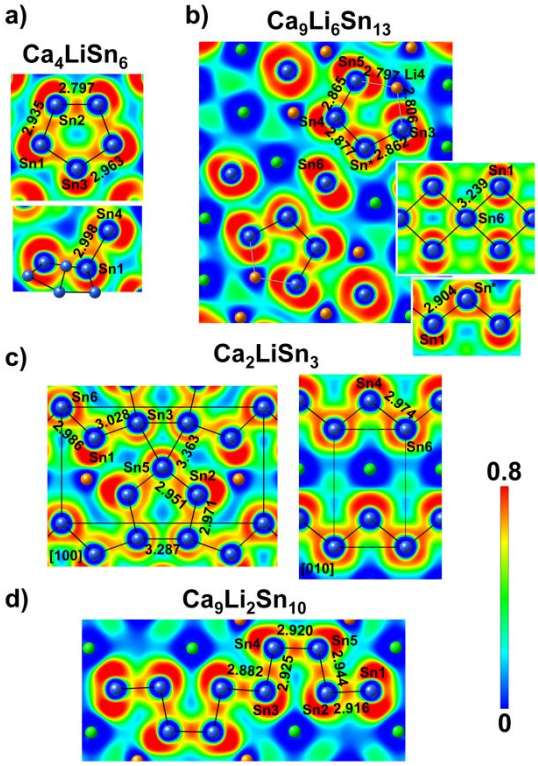

Figure 4. Selected sections of the crystal structures and Electron Localization Function (ELF) for Ca_4LiSn_6 (a), $Ca_9Li_6Sn_{13}$ (b), Ca_2LiSn_3 (c, the unit cell is outlined and crystal directions are indicated), and $Ca_9Li_2Sn_{10}$ (d).

Treating the (Li/Sn)3 and (Li/Sn)4 position of the original structure as Li and Sn, respectively, i.e., swapping the chemical types in the model, leads to the same idealized composition $Ca_9Li_6Sn_{13}$ and the same overall electron count, with a shortage of four electrons per formula unit. Although this electron count results from somewhat different formal charges of the Sn atoms, the electronic picture and conclusions regarding chemical bonding remain basically unchanged.

In the electronic structure of Ca_2LiSn_3, the Fermi level is located inside a sharp dip of the DOS, typical for metallic Zintl phases (Fig. 2c). Although such picture can be expected from the formal charge assigned proposed in the previous section, the chemical bonding in Ca_2LiSn_3 appears to be more complex (Fig. 3c). All calculated Sn–Sn interactions were found to be underoptimized at the Fermi level due to a partial occupation of antibonding states in the near vicinity of E_F. More specifically, the short Sn–Sn contacts with $d_{Sn–Sn}$ < 3.2 Å display predominantly bonding interactions below E_F and a comparably strong overall attraction, reflected an in average –ICOHP value of 1.47 eV/bond at the Fermi level. The long Sn–Sn contacts with $d_{Sn–Sn}$ = 3.287 Å and 3.363 Å both demonstrate significant contribution of antibonding interactions close to E_F, typical for hypervalent bonding, and highly reduced –ICOHP magnitudes of 0.47 and 0.26 eV/bond, respectively. In line with the COHP calculations, analysis of the ELF distribution suggests covalent character of bonding interactions for the shorter Sn–Sn contacts and the absence of two-electron interactions for the presumably hypervalent Sn–Sn bonds (Fig. 4c). The longest discussed Sn–Sn contact of 3.363 Å appears to have a non-negligible bonding contribution – an effect neglected in our formal charge assignment above. Nevertheless, the overall electronic picture suggests that the sophisticated combination of the covalent and hypervalent bonding in Ca_2LiSn_3 results in a state with the lowest DOS at the Fermi level, which probably explains the stability of this composition and the absence of any detectable homogeneity range.

The Fermi level in the electronic structure of the idealized defect-free $Ca_9Li_2Sn_{10}$ is situated just under a pseudogap located at $E – E_F \approx 0.25$ eV (Fig. 2d). This energy corresponds to one extra electron per formula unit of $Ca_9Li_2Sn_{10}$. As was discussed above, the treatment of the Sn–Sn bonding contacts as single bonds would result in the formal charge assignment $(Ca^{2+})_9(Li^+)_2(Sn^{2–})_8(Sn^{3–})_2(h^+)_2$, calling for two extra electrons to achieve charge balance. Considering a possible π-bonding involving the Sn3–Sn3 bond within the Sn_{10} chain, a fully electron-balanced notation results, $(Ca^{2+})_9(Li^+)_2(Sn^{1–})_2(Sn^{2–})_6(Sn^{3–})_2$. The real electronic distribution appears to be an intermediate state between these two possibilities, as suggested by the first-principle calculations. Based on these results, the formal charge of the Sn_{10} chain should be taken as "21–". The occurrence of π-bonding decreases the electron deficiency in the structure. In order to gain additional confirmation of the formal charge assignment, we performed first-principle calculations for a hypothetical isostructural compound $Ca_9LiMgSn_{10}$, which is expected to be electron-precise based on the above-given arguments. In line with this prediction, the Fermi level in the calculated model falls in a pseudogap in the electronic spectrum (Fig. S3). The π-bonding contribution in the chain explains the planarity of this structural moiety. Departure of the Sn–Sn interactions from ideal single bonding in $Ca_9Li_2Sn_{10}$ is also evident from the COHP calculations, showing partial population of antibonding states for the Sn–Sn contacts (Fig. 3d). The average Sn–Sn bonding remains quite strong with an –ICOHP value of 1.90 eV/bond. The strongly covalent nature of the homoatomic Sn interactions is also pronounced in the ELF distribution (Fig. 4d).

Experimental

Synthesis

All manipulations were performed in an argon-filled glovebox. Ca_4LiSn_6 and $Ca_9Li_{6+x}Sn_{13–x}$ ($x \approx 0.28$) were prepared using a Sn flux method. Elemental Ca, Li, and Sn (Alfa-Aesar, all with stated purity ≥ 99.9 wt. %) were loaded in alumina crucibles with the Ca:Li:Sn ratios of 2:1:5 (for the synthesis of Ca_4LiSn_6) and 1:1:3 (for the synthesis of $Ca_9Li_{6+x}Sn_{13–x}$, $x \approx 0.28$), respectively. The crucibles were topped with a piece of quartz wool, used as a filter for the eventual centrifugation, and sealed in evacuated fused silica tubes. The tubes were heated up to 523 K with a rate of 20 K/h, kept at this temperature for 3 h, after which the temperature was raised up to 1073 K at a rate of 50 K/h. After tempering the mixtures for 10 h, the reactors were cooled down to 773 K at a rate of 5 K/h. At this point, the tubes were taken out of the furnace, flipped over and subjected to centrifugation in order to remove the excess of the molten Sn. It is worthwhile to note that the reaction of Li with Sn produces a considerable amount of heat which can lead to shattering of the alumina crucibles. Therefore, the given experimental protocol included slow heating and pre-reaction of the mixtures at a temperature just above the melting point of Sn (T_m = 503 K). For both samples, significant losses of Li at high temperatures were observed due to side reactions with the reactor walls and the quartz wool filter.

Following the removal of molten flux, the tubes were brought back inside the glovebox and crack-opened; the produced crystals were mechanically extracted/separated with a pair of tweezers under a microscope. Visual inspection showed that well-formed cubic crystals were the main product for both starting compositions. Subsequent powder and single-crystal X-ray diffraction indicated that the cubic crystals belonged to the known binary compound $CaSn_3$.[14] However, a large number of small irregularly-shaped crystals were present in both samples along with $CaSn_3$. Crystal structure analysis revealed that these crystals were different for the two starting compositions. Namely, the sample with the elemental ratio Ca:Li:Sn = 2:1:5 yielded crystals with the refined composition Ca_4LiSn_6, whereas in the sample with the ratio Ca:Li:Sn = 1:1:3, crystals with the general formula $Ca_9Li_{6+x}Sn_{13–x}$ were identified. The presence of the new phases was also confirmed by powder X-ray diffraction of the ground samples.

After the composition of the two new compounds were determined, attempts were undertaken to prepare them as phase-pure materials using direct reaction of the elements in

weld-shut Nb tubes. However, these attempts produced two new compounds instead, indicating that the targeted compositions may be metastable. The two new compositions discovered in the Nb tube reactions were Ca_2LiSn_3 and $Ca_{9-x}Li_2Sn_{10}$ ($x \approx 0.16$). The following optimized synthetic procedure allowed production of these two compositions as major phases. The elements were loaded in the Nb tubes with the ratios Ca:Li:Sn = 2:1:3 and 9:2:10, respectively. The tubes were weld-shut under high-purity Ar using an arc-welder and enclosed in evacuated fused silica tubes. After heating up to 1073 K with a rate of 200 K/h and holding at this temperature for 48 h, the reactors were cooled down to room temperature with a rate of 5 K/h. The resulting samples were well-crystalline grey powders.

Powder X-ray diffraction (PXRD)

PXRD measurements were conducted at room temperature on a Rigaku Miniflex diffractometer (filtered Cu Kα radiation, λ = 1.5418 Å) operating inside a nitrogen-filled glovebox. This allowed the data collection for samples, which decompose quickly in air. Data were collected in a Θ–Θ scan mode between 5° and 75° with a step size of 0.05° and 2 s/step counting time. Powder diffraction patterns for the samples with nominal compositions "Ca_2LiSn_3" and "$Ca_9Li_2Sn_{10}$" prepared in Nb tubes are shown in Fig. S1 in ESI.

Single-crystal X-ray diffraction (SCXRD)

Suitable single crystals were selected in the glovebox and cut with a scalpel under dry Paratone N oil. The chosen specimens were scooped from the oil droplet oil using low-background plastic loops. The crystals were protected from the ambient atmosphere in a cold nitrogen stream. Data collection was accomplished with the aid of a Bruker SMART CCD-diffractometer, equipped with monochromated Mo Kα radiation (λ = 0.71073 Å). The raw data were integrated using the program SAINT.[37] Semi-empirical absorption corrections were applied with the SADABS software.[38] Crystal structures were solved by direct methods as implemented in SHELXT,[39] and refined by full matrix least-squares methods on F^2 using SHELXL.[40] Atomic labelling and coordinates were standardized using STRUCTURE TIDY.[41] Details of the data collection, crystallographic parameters, and selected interatomic distances are summarized in Tables 1–5 and S1–S4 (ESI).

Table 1 Data collection details and crystallographic data (T = 200 K, Mo Kα, λ = 0.71073 Å)

Refined composition	Ca_4LiSn_6	$Ca_9Li_{6.28(1)}Sn_{12.72}$	Ca_2LiSn_3	$Ca_{8.84(1)}Li_2Sn_{10}$
Formula weight/ g mol^{-1}	879.40	1913.48	443.17	1555.29
Space group	*Pbcm*, Z = 4	*C*2/*m*, Z = 2	*Pmm*2, Z = 3	*C*2/*m*, Z = 2
a/ Å	9.2035(4)	17.210(2)	4.6391(9)	22.547(2)
b/ Å	8.8019(5)	4.6081(6)	13.3172(6)	4.7638(5)
c/ Å	14.9400(8)	18.881(2)	7.652(2)	11.487(1)
β/ °	-	107.810(2)	-	101.603(1)
V/ Å^3	1210.3(1)	1425.6(3)	472.7(1)	1208.6(2)
ρ_{calc}/ g cm^{-3}	4.83	4.46	4.67	4.27
$\mu_{MoK\alpha}$/ cm^{-1}	138.2	125.3	132.7	120.0
R_1 [$I > 2\sigma(I)$][a]	0.017	0.035	0.031	0.018
wR_2 [all data][a]	0.036	0.078	0.065	0.040
$\Delta\rho_{max,min}$/ e Å^{-3}	0.97, –0.67	1.64, –1.71	2.02, –2.15	0.95, –0.90

[a] $R1 = \sum||F_o|-|F_c||/\sum|F_o|$; $wR_2 = [\sum[w(F_o^2-F_c^2)^2]/\sum[w(F_o^2)^2]]^{1/2}$, where $w = 1/[\sigma^2F_o^2+(A\cdot P)^2+(B\cdot P)]$, and $P = (F_o^2+2F_c^2)/3$; *A, B* are the respective weight coefficients (see CIF in the supporting information). CIFs have been deposited with reference numbers CCDC 1938687-1938690

Table 2 Atomic coordinates and equivalent isotropic displacement parameters (U_{eq}[a]) for Ca_4LiSn_6

Atom	Site	*x*	*y*	*z*	U_{eq}/ Å^2
Ca1	8*e*	0.12107(7)	0.39671(8)	0.10905(5)	0.0131(2)
Ca2	4*d*	0.7434(1)	0.2666(1)	1/4	0.0135(2)
Ca3	4*c*	0.5122(1)	1/4	0	0.0122(2)
Li1	4*d*	0.3739(9)	0.210(1)	1/4	0.016(2)
Sn1	8*e*	0.24995(2)	0.03242(3)	0.08824(2)	0.01115(8)
Sn2	8*e*	0.45439(3)	0.48538(3)	0.15639(2)	0.01146(8)
Sn3	4*d*	0.07615(3)	0.10267(4)	1/4	0.01088(9)
Sn4	4*c*	0.86251(4)	1/4	0	0.0181(1)

[a] U_{eq} is defined as one third of the trace of the orthogonalized U_{ij} tensor.

Table 3 Atomic coordinates and equivalent isotropic displacement parameters (U_{eq}[a]) for $Ca_9Li_{6+x}Sn_{13-x}$ (x = 0.28(1))

Atom	Site	*x*	*y*	*z*	U_{eq}/ Å^2
Ca1	4*i*	0.0700(1)	0	0.6347(1)	0.0146(4)
Ca2	4*i*	0.0877(1)	0	0.2364(1)	0.0148(4)
Ca3	4*i*	0.2806(1)	0	0.4238(1)	0.0163(5)
Ca4	4*i*	0.8567(1)	0	0.1332(1)	0.0160(4)
Ca5	2*a*	0	0	0	0.0128(6)
Li1	4*i*	0.283(1)	0	0.2385(9)	0.017(4)
Li2	4*i*	0.334(1)	0	0.007(1)	0.028(5)
(Li/Sn)3[b]	4*i*	0.60938(8)	0	0.37147(7)	0.0139(4)
(Li/Sn)4[b]	4*i*	0.6583(1)	0	0.1436(1)	0.0151(7)
Sn1	4*i*	0.11654(4)	0	0.46684(4)	0.0155(2)
Sn2	4*i*	0.20723(4)	0	0.07893(4)	0.0142(2)
Sn3	4*i*	0.26757(4)	0	0.70177(4)	0.0150(2)

Sn4	4*i*	0.45506(4)	0	0.25577(4)	0.0126(2)
Sn5	4*i*	0.48913(4)	0	0.11645(4)	0.0122(2)
Sn6	2*d*	0	1/2	1/2	0.0166(2)

[a] U_{eq} is defined as one third of the trace of the orthogonalized U_{ij} tensor; [b] (Li/Sn)3 = 0.455(3)Li + 0.545Sn, (Li/Sn)4 = 0.687(3)Li + 0.313Sn.

Table 4 Atomic coordinates and equivalent isotropic displacement parameters (U_{eq}[a]) for Ca_2LiSn_3

Atom	Site	*x*	*y*	*z*	U_{eq}/ Å^2
Ca1	2*h*	1/2	0.2116(3)	0.0249(5)	0.0093(9)
Ca2	2*h*	1/2	0.2963(4)	0.5377(6)	0.017(1)
Ca3	1*d*	1/2	1/2	0.1500(9)	0.012(1)
Ca4	1*c*	1/2	0	0.6609(9)	0.015(1)
Li1	2*g*	0	0.126(3)	0.37(1)	0.02(1)[b]
Li2	1*d*	1/2	1/2	0.73(1)	0.02[b]
Sn1	2*g*	0	0.1626(1)	0.7314(2)	0.0094(4)
Sn2	2*g*	0	0.32585(9)	0.2434(2)	0.0087(3)
Sn3	2*g*	0	0.3766(1)	0.8653(3)	0.0103(3)
Sn4	1*c*	1/2	0	0.2433(4)	0.0126(4)
Sn5	1*b*	0	1/2	0.4819(3)	0.0104(5)
Sn6	1*a*	0	0	0.0001(3)	0.0186(6)

[a] U_{eq} is defined as one third of the trace of the orthogonalized U_{ij} tensor; [b] Li1 and Li2 were refined isotropically and their U_{iso} were set to be equal.

Table 5 Atomic coordinates and equivalent isotropic displacement parameters (U_{eq}[a]) for $Ca_{9-x}Li_2Sn_{10}$ (x = 0.16(1))

Atom	Site	*x*	*y*	*z*	U_{eq}/ Å^2
Ca1	4*i*	0.05516(3)	0	0.65052(6)	0.0110(1)
Ca2	4*i*	0.10531(3)	0	0.30789(7)	0.0118(1)
Ca3	4*i*	0.20805(3)	0	0.09185(6)	0.0108(1)
Ca4	4*i*	0.30477(3)	0	0.40252(7)	0.0123(1)
Ca5[b]	2*a*	0	0	0	0.0139(4)
Li1	4*i*	0.3689(3)	0	0.1334(6)	0.018(1)
Sn1	4*i*	0.19131(2)	0	0.80240(2)	0.01016(6)
Sn2	4*i*	0.29465(2)	0	0.68522(2)	0.01022(6)
Sn3	4*i*	0.44453(2)	0	0.54418(2)	0.00997(6)
Sn4	4*i*	0.49905(2)	0	0.20321(2)	0.01051(6)
Sn5	4*i*	0.60780(2)	0	0.10164(2)	0.01033(6)

[a] U_{eq} is defined as one third of the trace of the orthogonalized U_{ij} tensor; [b] Ca5 occupancy is 0.843(5).

Electronic structure calculations

Electronic structures were evaluated using the TB-LMTO-ASA program package.[42] All calculations were done within the local density approximation using the von Barth-Hedin implementation of the exchange-correlation functional.[43] To satisfy the Atomic Sphere Approximation (ASA), an introduction of empty spheres was necessary. For the analysis of chemical bonding, Crystal Orbital Hamilton Population curves (COHP) and Electron Localization Function (ELF) were generated using the dedicated modules in LMTO.

Conclusions

Four new ternary compounds in the system Ca–Li–Sn have been structurally characterized and analyzed using first-principle calculations. Each of the new compositions crystallize in its own structure type with complex polyanionic structural units based on Sn. Ca_4LiSn_6 displays single-bonded Sn–Sn interactions and reveals a shortage of one electron per formula unit with respect to a charge-balanced count. In contrast, an almost electron-precise formulation is achieved in $Ca_9Li_{6+x}Sn_{13-x}$ ($x \approx 0.28$) due to a peculiar disorder and combination of covalent and hypervalent Sn–Sn bonding. A similarly complex interplay of different kinds of homoatomic Sn–Sn interactions in the disorder-free Ca_2LiSn_3 results in a stable electronic structure with a sharp dip in the DOS at the Fermi level. The crystal structure of $Ca_{9-x}Li_2Sn_{10}$ ($x \approx 0.16$) features infinite chains, where the Sn–Sn bonding can be understood as a combination of single- and double-bonds. The resulting formal charge of the repeating $[Sn_{10}]$-unit is "21–", as also indicated by the first-principle calculations. In the cationic substructure, there is a small deficiency of Ca in one of the crystallographic sites, probably related to entropy factors. The new compounds can be potentially interesting for electrochemical testing owing to their expected metallic properties.

Conflicts of interest

There are no conflicts to declare.

Acknowledgements

This work was supported by the National Science Foundation under Award # NSF DMR-1709813. The authors also thank Dr. S.-P. Guo for conducting some preliminary work in the Ca–Li–Sn system and discovering the phase Ca_2LiSn_3.

Notes and references

1 J. B. Goodenough and Y. Kim, *Chem. Mater.*, 2010, **22**, 587–603.

2 S. Goriparti, E. Miele, F. De Angelis, E. Di Fabrizio, R. Proietti Zaccaria and C. Capiglia, *J. Power Sources*, 2014, **257**, 421–443.

3 Y. Li, R. Raghavan, N. A. Wagner, S. K. Davidowski, L. Baggetto, R. Zhao, Q. Cheng, J. L. Yarger, G. M. Veith, C. Ellis-Terrell, M. A. Miller, K. S. Chan and C. K. Chan, *Adv. Sci.*, 2015, **2**, 1500057.

4 R. Zhao, S. Bobev, L. Krishna, T. Yang, J. M. Weller, H. Jing and C. K. Chan, *ACS Appl. Mater. Interfaces*, 2017, **9**, 41246–41257.

5 A. Dopilka, R. Zhao, J. M. Weller, S. Bobev, X. Peng and C. K. Chan, *ACS Appl. Mater. Interfaces*, 2018, **10**, 37981–37993.

6 M. Xue and Z. Fu, *Solid State Ion.*, 2006, **177**, 1501–1507.

7 M. M. Thackeray, J. T. Vaughey, A. J. Kahaian, K. D. Kepler and R. Benedek, *Electrochem. Commun.*, 1999, **1**, 111–115.

8 J. T. Vaughey, K. D. Kepler, R. Benedek and M. M. Thackeray, *Electrochem. Commun.*, 1999, **1**, 517–521.

9 T. Kosho, K. Kishida, K. Tanaka and H. Inui, *Adv. Mater. Res.*, 2007, **26–28**, 225–228.

10 A. Ovchinnikov and S. Bobev, *Inorg. Chem.*, 2019, **58**, 7895–7904.

11 W. Müller and R. Voltz, *Z. Naturforsch. B*, 1974, **29**, 163–165.

12 I. Todorov and S. C. Sevov, *Inorg. Chem.*, 2005, **44**, 5361–5369.

13 D. Stoiber, M. Bobnar, P. Höhn and R. Niewa, *Z. Naturforsch. B*, 2017, **72**, 847–853.

14 E. Zintl and S. Neumayr, *Z. Elektrochem.*, 1933, **39**, 86–97.

15 I. Todorov and S. C. Sevov, *Inorg. Chem.*, 2004, **43**, 6490–6494.

16 R. Pöttgen, *Z. Naturforsch. B*, 2006, **61**, 677–698.

17 T. F. Fässler, Ed., *Zintl Phases*, Springer Berlin Heidelberg, Berlin, Heidelberg, 2011, vol. 139.

18 R. Nesper, *Z. Anorg. Allg. Chem.*, 2014, **640**, 2639–2648.

19 A. Ovchinnikov and S. Bobev, *J. Solid State Chem.*, 2019, **270**, 346–359.

20 R. J. Wilson, B. Weinert and S. Dehnen, *Dalton Trans.*, 2018, **47**, 14861–14869.

21 X. He, Y. Fu, D. J. Singh and L. Zhang, *J. Mater. Chem. C*, 2016, **4**, 11305–11312.

22 D. O. Ojwang and S. Bobev, *Inorganics*, 2018, **6**, 109.

23 T.-S. You and S. Bobev, *J. Solid State Chem.*, 2010, **183**, 2895–2902.

24 J. P. A. Makongo and S. Bobev, *Acta Crystallogr. C*, 2014, **70**, 2–6.

25 T. L. Reichmann, C. Gebert and D. M. Cupid, *J. Alloys Compd.*, 2017, **714**, 593–602.

26 G. R. Goward, N. J. Taylor, D. C. S. Souza and L. F. Nazar, *J. Alloys Compd.*, 2001, **329**, 82–91.

27 J. P. A. Makongo, N.-T. Suen, S. Guo, S. Saha, R. Greene, J. Paglione and S. Bobev, *J. Solid State Chem.*, 2014, **211**, 95–105.

28 G. A. Papoian and R. Hoffmann, *Angew. Chem. Int. Ed.*, 2000, **39**, 2408–2448.

29 A. L. Spek, *Acta Crystallogr. D*, 2009, **65**, 148–155.

30 H. T. Stokes and D. M. Hatch, *J. Appl. Crystallogr.*, 2005, **38**, 237–238.

31 L. Pauling, *The Nature of the Chemical Bond*, Cornell Univ. Press, Ithaca, New York, 1960.

32 S. Wengert and R. Nesper, *Z. Für Anorg. Allg. Chem.*, 1998, **624**, 1801–1806.

33 W. Carrillo-Cabrera, S. Budnyk, Y. Prots and Y. Grin, *Z. Anorg. Allg. Chem.*, 2004, **630**, 2267–2276.

34 R. Castillo, W. Schnelle, M. Bobnar, U. Burkhardt, B. Böhme, M. Baitinger, U. Schwarz and Y. Grin, *Z. Anorg. Allg. Chem.*, 2015, **641**, 206–213.

35 A. Ovchinnikov and S. Bobev, *Acta Crystallogr. C*, 2018, **74**, 269–273.

36 A. Ovchinnikov and S. Bobev, *Acta Crystallogr. C*, 2018, **74**, 618–622.

37 *SAINT, Bruker AXS Inc., Madison, Wisconsin, USA, 2014*.

38 *SADABS, Bruker AXS Inc., Madison, Wisconsin, USA, 2014*.

39 G. M. Sheldrick, *Acta Crystallogr. Sect. Found. Adv.*, 2015, **71**, 3–8.

40 G. M. Sheldrick, *Acta Crystallogr. Sect. C Struct. Chem.*, 2015, **71**, 3–8.

41 L. M. Gelato and E. Parthé, *J. Appl. Crystallogr.*, 1987, **20**, 139–143.

42 O. Jepsen and O. K. Andersen, The Stuttgart TB-LMTO-ASA Program, Version 4.7; Max-Planck-Institut für Festkörperforschung: Stuttgart, Germany.

43 U. von Barth and L. Hedin, *J. Phys. C Solid State Phys.*, 1972, **5**, 1629–1642.

Four new ternary phases in the system Ca–Li–Sn have been prepared and characterized using single-crystal X-ray diffraction and first-principle calculations. The new compounds demonstrate rich diversity of Sn-based polyanionic structures with various chemical bonding patterns.